Neurobiology of Aging 69 (2018) 261–273

Contents lists available at ScienceDirect

Neurobiology of Aging

journal homepage: www.elsevier.com/locate/neuaging

Aging of human alpha rhythm

Maria G. Knyazeva [a,b,*], Elham Barzegaran [a,b], Vladimir Y. Vildavski [c], Jean-François Demonet [b]

[a] Department of Clinical Neurosciences, Laboratoire de recherche en neuroimagerie (LREN), Lausanne University Hospital and University of Lausanne, Lausanne, Switzerland
[b] Department of Clinical Neurosciences, Leenaards Memory Centre, Centre Hospitalier Universitaire Vaudois and University of Lausanne, Lausanne, Switzerland
[c] Department of Psychology, Stanford University, Stanford, CA, USA

ARTICLE INFO

Article history:
Received 9 October 2017
Received in revised form 11 May 2018
Accepted 12 May 2018
Available online 22 May 2018

Keywords:
Alpha rhythm slowing
Component structure of alpha rhythm
Oscillations
PARAFAC
Resting state
Source localization

ABSTRACT

Alpha rhythm (AR) changes are the most pronounced electroencephalogram phenomenon in the aging brain. We analyzed them based on the inherent AR structure obtained by parallel factor analysis decomposition in the cortical source space. AR showed a stable multicomponent structure in 78% of sixty 20- to 81-year-old healthy adults. Typically, it consists of 2 components. The distribution of the higher frequency occipito-parietal component widens with age, with its maximum moving from BA18/19 to BA37. The low-frequency component originating from the occipito-temporal regions in young adults also moves anteriorly with age, while maintaining its maximum within BA37. Both components slow down by 1 Hz over the adult lifespan. The multicomponent AR is more common in younger subjects, whereas a single-component AR in older subjects. This uneven occurrence as well as the increasing spatial and frequency overlaps between components suggest transformation of the multicomponent AR into the single-component AR with age. A detailed knowledge of AR component structure would be useful to monitor age-related neurodegenerative processes in humans.

1. Introduction

The changes of the posterior alpha rhythm (AR) in electroencephalogram (EEG) are among the most pronounced phenomena related to brain aging in humans. They include AR slowing (Başar, 2012; Clark et al., 2004; Gaál et al., 2010; Hubbard et al., 1976; Lodder and van Putten, 2011; Markand, 1986; Peltz et al., 2010; Shigeta et al., 1995; Van Sweden et al., 1999; Wang and Busse, 1969), reduction of its power (Lodder and van Putten, 2011; Vysata et al., 2012), a shift of AR sources in the posterior-to-anterior direction (Babiloni et al., 2006; Niedermeyer, 1997; Rossini et al., 2006), and the declining AR reactivity (Gaál et al., 2010; Hong et al., 2015; Vaden et al., 2012) observed in middle-aged and older participants.

The description of age-related AR changes has been largely based on the analysis of the entire AR band or AR peak (Caplan et al., 2015; Davidson and Davidson, 2012; Peltz et al., 2010). Alternatively, some studies reported differential effects of aging on *pre-selected* high- and low-frequency sub-bands of AR (Babiloni et al., 2015; Moretti et al., 2004). However, these findings have only limited explanatory potential, as the correspondence of fixed sub-bands to separate rhythmic components remains an open question.

The concept of individual AR peak frequency (Klimesch, 1999) became an essential step toward improved AR analysis. The evidence-supported alpha sub-bands (i.e., having borders dependent on the individual peak frequency) correlated better with neurodegeneration in the older adults than the fixed ones (Angelakis et al., 2007; Moretti et al., 2011). Yet, this procedure cannot reveal the inherent structure of the AR. The variation in the number (2 or 3) of analyzed sub-bands among published reports once again emphasizes the subjective nature of such segmentation.

Meanwhile, it is essential to consider the number, origin, and functionality of the rhythms that contribute to the posterior AR in the surface EEG for understanding its evolution with age. Indeed, in the presence of more than 1 component, characterized by individual frequency, source, and temporal dynamics, the age-related AR changes, stated previously, can be explained by different scenarios. For instance, the observed slowing down of the posterior AR with age may result from a decrease in the frequency of all AR components, or from a decrease in the power of the high-frequency component, leading to different interpretations of aging processes in the brain.

* Corresponding author at: Department of Clinical Neurosciences, Lausanne University Hospital and University of Lausanne, 1011 Lausanne, Switzerland. Tel.: +41 21 314 32 31.
E-mail address: mariagknyazeva@gmail.com (M.G. Knyazeva).

0197-4580/$ – see front matter © 2018 Elsevier Inc. All rights reserved.
https://doi.org/10.1016/j.neurobiolaging.2018.05.018

An inherent structure of the AR can be demonstrated by its decomposition with a multidimensional technique that takes into account all 3 natural EEG dimensions—time, space, and frequency. To this end, by using a 3-way parallel factor analysis (PARAFAC) method, we found a stable multicomponent AR structure in about 90% of *young healthy adults* (Barzegaran et al., 2017). In addition to the predominant occipito-parietal component of AR, well known from the literature, we identified a weaker occipito-temporal component, largely left unattended in previous studies. These 2 components comprised the most typical configuration of the posterior AR, recordable with noninvasive surface EEG in young adults.

Building upon our findings regarding AR structure in young people and the aforementioned phenomenology of AR changes in the older adults, we suggest that each of the AR components has its own evolution, leading to the distortion of AR structure with age. We test this hypothesis by identifying the AR structure of middle-aged to older normal adults with the PARAFAC method, comparing it to that of young participants and, finally, analyzing the age-related trends over the adult lifespan.

2. Methods

2.1. Participants

In this study, we analyzed EEG data of 60 participants aged from 20 to 81 years. The data from healthy 20- to 45-year-old participants, representing AR structure in early adulthood, have recently been reported (Barzegaran et al., 2017) and are used here only to characterize AR evolution over the adult lifespan (see Section 2.9).

Thirty-two middle- to old-aged community-dwelling adults were de novo enrolled in the study. Potential participants underwent a brief clinical interview that included the Montreal Cognitive Assessment (MoCA) test. The description of AR structure in the aging population is based on EEG data from these individuals (12 men and 20 women aged 45–81 years) with a MoCA score $\geq$26 (mean group score was 27.4) and without cognitive complaints, past or present neurological or psychiatric illness including depression, psychoactive drug use or alcohol use disorders, head trauma, chronic systemic illnesses or other conditions that interfere with cognition (for details see Supplementary materials, Section I).

According to the Hospital Anxiety and Depression scale (Zigmond and Snaith, 1983), none of the recruited participants showed symptoms of depression as indicated by the individual scores all being <8. Independent living skills of all the potential participants aged 65+ years had been assessed with the Lawton Instrumental Activities of Daily Living Scale (Lawton and Brody, 1969). At the time of experiment, all the actual participants functioned independently in the 8 (women) or 5 (men) domains of function included in the Instrumental Activities of Daily Living scale.

The sample selected using abovementioned tests represents adults without clinically significant evidence of brain pathology, that is, those in the course of *normal aging* in contrast to *healthy or successful aging*. The latter is characterized by the uncommon structural and functional preservation of the brain that can be shown with extended neuropsychological and neurological examinations and brain imaging (Harrison et al., 2012; Rogalski et al., 2013, 2018). Our choice of tests and inclusion/exclusion criteria for participants of this study was motivated by the objective to explore *typical age-related changes of the inherent AR structure* rather than exceptional neuroprotective mechanisms that stand against destructive aspects of aging.

All methods and procedures in this study conform to the Declaration of Helsinki (1964) of the World Medical Association concerning human experimentation (Rickham, 1964). It was also approved by the local Ethics Committee (Commission cantonale d'éthique de la recherche sur l'être humain). We provided the essential information about the research to each potential participant and obtained written informed consent from all actual participants.

2.2. EEG recording and preprocessing

Here, we briefly summarize methods used for collecting and analyzing EEG data. For detailed technical description, the reader is referred to Barzegaran et al. (2017). The recording sessions of 90–120 minutes included several cognitive tasks and Rest with Eyes Open (REO) interleaved with the Resting state with Eyes Closed (REC). Detailed description of the recording timeline is presented in Supplementary materials, Section II. We concatenated the REC or REO episodes (each $\leq$3 minutes) into 4 consecutive REC periods and 1 REO period of 8–10 minutes. This report is mainly based on the data from all 4 REC periods (REC1–REC4). The REO condition was used to analyze the AR reactivity (Supplementary materials, Section III).

The EEGs were collected on a 64-channel mobile EEG system eego sports using waveguard original electrode caps (ANT Neuro, Enschede, The Netherlands) with a CPz reference and a high-cutoff filter set to 100 Hz. The electrode impedances were kept under 30 kΩ (under 10 kΩ in most cases), which was well below the recommended maximum of 50 kΩ for high-impedance eego amplifiers. The EEGs were digitized at 500 Hz with a 24-bit resolution and band-pass filtered within a 1- to 45-Hz band by a phase preserving digital filter. We marked the artifacts based on the off-line visual inspection and used the data without visible artifacts for further analysis. We removed the 2 mastoid electrodes, which contained low-quality EEG in many participants from the data before re-referencing the signals from CPz to the common average of the remaining electrodes.

2.3. General design of EEG analysis

A multidimensional 3-way PARAFAC, breaking the source-space EEGs into a number of AR components (ARCs), lies at the core of the data processing in this study. We calculated the time-varying spectra of the scalp EEGs by taking short-term Fourier transforms over a large number of epochs (see Section 2.4), and then converted the spectra to the cortical space by the low-resolution electromagnetic tomography technique (Section 2.5). We applied the first PARAFAC decomposition to the sensor-space spectra, yielding reliable estimates of the frequency, space, and time features of the components (Section 2.6). In the second application of the PARAFAC to the cortical-space spectra, we took the frequency and time features as fixed parameters from the sensor-space decomposition, thus reducing the number of estimated parameters and obtaining robust estimates of the cortical distribution of the components. We then characterized the ARCs statistically (Section 2.7) including the assessment of their temporal stability (Section 2.8), as well as age-related trends (Section 2.9). For more details and the block diagram of the analysis design, we refer the reader to Barzegaran et al. (2017).

2.4. Spectral analysis of EEG

We calculated the time-frequency representation of multichannel EEG signals from all 4 REC periods by the discrete short-time Fourier transform of 5-second artifact-free epochs multiplied by the Hann window and overlapped by 50%. For the REC condition, the number of time windows constituted 782 $\pm$ 114 (mean $\pm$ standard deviation), while for REO it was 182 $\pm$ 63 per participant.

The electrode-space cross-spectrum density matrix CSD_{φ} ($N_e \times N_e \times N_f \times N_t$), where N_e is the number of electrodes, was calculated through multiplication of spectral matrix by its complex conjugate with subsequent normalization. The frequency N_f and time N_t dimensions of the cross-spectrum matrix represent the 5–15 Hz extended alpha range and the number of time windows covering combined REC interval and are sampled with the $df = 0.2$ Hz and the $dt = 2.5$ seconds resolution, respectively. The amplitude spectral density (ASD) $ASD\varphi_{f,t}$ at frequency f and time t was calculated for each electrode as a square root of the diagonal of $CSD\varphi_{f,t}$, and we used the amplitude spectrum matrix ASD_{φ} ($N_e \times N_f \times N_t$) as the input for the first PARAFAC.

2.5. Source-space EEG analysis

We obtained cortical distribution of the EEG spectra using low-resolution electromagnetic tomography inverse solution (Pascual-Marqui et al., 1994) with a lead field matrix calculated for the MNI (Montreal Neurological Institute) 152 average brain (Fonov et al., 2009) and a 3-shell locally spherical model with anatomical constraints with 3005 uniformly distributed sources. The resulting inverse matrix T was downsampled to 387 uniformly distributed sources, and we computed the source cross-spectrum at frequency f and time t, $CSDj_{f,t}$ ($N_S \times N_S$) as a projection of the sensor-space cross-spectrum $CSD\varphi_{f,t}$ to the cortical space using the down-sampled inverse matrix, where N_S is the number of sources. Similar to the sensor-space data, the square root of the CSD_j diagonal represents the amplitude spectral density ASD_j ($N_s \times N_f \times N_t$) for each cortical location.

2.6. Parallel factor analysis

Our main findings are based on the decomposition of the EEG alpha band into a small number of components, characterized by their frequencies, cortical distributions, and temporal dynamics, with a 3-way PARAFAC technique. Being a generalization of the Principle Component Analysis to higher order data (Bro, 1997; Carroll and Chang, 1970; Harshman, 1970), the PARAFAC yields a unique solution, given a correct number of components and a sufficiently high signal-to-noise ratio. We used the N-way MATLAB toolbox (Andersson and Bro, 2000) as a PARAFAC implementation. In our case, this solution represents the original multidimensional amplitude EEG spectra as a sum of components in the following form:

$$ASD_{e,f,t} = \sum_{k=1}^{K} A_{ek} B_{fk} C_{tk} + \varepsilon_{e,f,t}\ , \qquad (1)$$

where $ASD_{e,f,t}$ is an element of the 3-way matrix ASD at electrode/source e, frequency f, and time window t, and A_{ek}, B_{fk}, and C_{tk} are the elements of the loading matrices A, B, and C that correspond to the space (electrodes or sources), frequency, and time dimensions of the original data with $\varepsilon_{e,f,t}$ being the error term of the decomposition. The columns of each loading matrix represent "signatures" of the components in the corresponding dimension.

Because PARAFAC is sensitive to the number of estimated parameters and the signal-to-noise ratio, we first applied it to the sensor-space amplitude spectra ASD_{φ} and obtained reliable estimates of the frequency and temporal features of the components. Then, using these estimates as fixed parameters, we applied the PARAFAC decomposition to the source-space spectra, ASD_j, thus, providing the cortical distributions of ARCs represented by the spatial loadings of the components. The spatial extent and the foci of the components are described in terms of the Brodmann atlas of cortical areas.

Our choice of the number of components, which is an important part of the PARAFAC decomposition, was guided by the CORe CONsistency DIAgnostic test implemented in the N-way toolbox (Bro and Kiers, 2003; Field and Graupe, 1991). The core consistency values, which vary from 0% (or <0%) for invalid models to 100% for a perfect model, were calculated for several models with different number of components, and a model with the highest number of components and the core consistency higher than a 90% threshold was chosen as a valid model. More details of model validation are presented in Barzegaran et al. (2017). The components with broadband flat spectra and those with spectra dominated by the low-frequencies and the highest loadings on frontal and anterior temporal regions have been removed from further analysis; as such, components most likely represented the muscle and ocular artifacts.

In theory, the PARAFAC analysis of the whole-head EEG should be able to identify not only posterior ARCs but the central mu rhythm as well. However, in practice, as we showed previously (Barzegaran et al., 2017), detection of the mu rhythm requires special adjustments of the technique, in particular, limiting the data to EEGs from only central and paracentral electrodes. Because the source reconstruction of the posterior AR required the whole-head PARAFAC, the mu rhythm remained undetected.

2.7. Statistical characterization of ARCs

We described ARCs in terms of their frequency features (peak, width, and overlap), distribution in the cortical source space, and stability on the 2 temporal scales (minutes to hours and weeks to months). Following the notation in (Barzegaran et al., 2017), for participants with 2 ARCs, the higher frequency ARC is labeled ARC1 and the lower frequency one, ARC2.

The peak frequency of ARC was defined as the frequency with maximum loading vector. The width of ARC was determined at the half-maximum of the frequency loading. The overlap between ARC1 and ARC2 was calculated as $\frac{W_1+W_2}{P_1-P_2}$ where W_1, P_1, W_2, and P_2 are the width and peak frequency of ARC1 and ARC2, respectively. The ARC amplitude ratio was calculated as ARC1/ARC2 using respective ASD values at a frequency with maximum frequency loading and maximum spatial loading.

The source distributions of ARC1 and ARC2 were contrasted using a cluster-based permutation test (Maris and Oostenveld, 2007) applied to their spatial loadings. This nonparametric method determines the largest significant cluster that survived corrections for multiple comparisons. Here, for each source, we extracted t-statistic by applying a one-sided paired t-test to the ARC1 and ARC2 loading values. We then calculated the cluster statistics as the sum of supra-threshold t-statistics of adjacent sources. The supra-threshold values were defined as t-values larger than the 99th percentile of t-distribution. The largest cluster statistics was then determined as the cluster statistics related to the largest cluster. The ARC labels were permuted 5000 times and, for each permutation, we extracted the largest cluster statistics. Finally, we calculated the p-value for the largest cluster as the proportion of cluster statistics in their random distribution larger than the non-permuted cluster statistic to the total number of permutations.

2.8. Assessment of temporal stability of ARCs

We tested the temporal dynamics of ARCs in each EEG session by calculating mean temporal loadings of ARC1 and ARC2, normalized to have maximum value of 1, over each of the 4 REC periods. Follow-

up EEG sessions implemented 2–20 months after the baseline recordings allowed us to estimate the stability of the AR structure on a "months-to-years" time scale in 8 middle-aged and older participants [see Barzegaran et al. (2017) for the respective data on young adults]. The individual temporal stability of the spatial and frequency features of ARCs was estimated by the similarity of loading vectors in the 2 recordings using the Tucker Congruence Coefficient (TCC), which varies between 0 and 1 for non-negative loadings (Lorenzo-Seva and Ten Berge, 2006). A value of $0.85 < TCC \leq 0.95$ corresponds to highly similar loading vectors, while $TCC > 0.95$, to virtually equal ones.

2.9. Regression analysis of age-related trends

The choice of regression as a method of analysis is defined by the continuous process of brain aging, which manifests itself in the gradual accumulation of age-related effects without clear leaps or stages due to various aging trajectories of different functional and structural parameters: some of those remain stable until the 7th decade of life, while others begin to decline as early as in 20s and 30s (Fotenos et al., 2005; Ge et al., 2002; Launer, 2005; Lockhart and DeCarli, 2014; Pfefferbaum et al., 2013; Raz et al., 2005; Salthouse, 2009; Singh-Manoux et al., 2012; Whalley et al., 2006). To examine the effects of aging on the multicomponent AR structure, we used the data from all participants with at least 2 ARCs, while excluding 2 outliers with ARC1 peak frequency outside the 2 standard deviation region. We applied a linear regression analysis to each of the above-defined ARC characteristics as dependent variables, using age as an independent variable. We also examined the effect of age on the source distribution of ARCs. To this end, loading vectors for each participant and ARC were normalized such that their sum was equal to 1 (to minimize the inter-individual variability) and log-transformed (to obtain a normal distribution of residuals). We then applied a linear regression analysis to these normalized loadings of ARC1 and ARC2 in each source of all available participants. The statistical significance of the results was determined with a cluster-based permutation test (see Section 2.7) applied to the source-wise F-statistics extracted from the regression analyzes. We also documented the "movement" of the ARC peak frequency coordinates in the MNI space with age. The peak frequency locations on lateral (medial-to-lateral direction), medial (posterior-to-anterior direction), and axial (inferior-to-superior) axes of the brain were regressed on age.

3. Results

3.1. AR structure in middle-aged and older participants

Similar to young adults (Barzegaran et al., 2017), the middle-aged and older participants typically (21 participants out of 32) showed a 2-component structure of the AR (Fig. 1A). The higher frequency component (ARC1) had an average peak frequency of 9.9 $\pm$ 0.8 Hz, and the lower frequency component (ARC2) had an average frequency of 9.0 $\pm$ 0.9 Hz. Both components were widely distributed over the posterior cortices (Fig. 2). We localized the group maxima of their cortical distributions to the BA37. Although the ARC2 maximum was located more anteriorly and laterally than that of ARC1, (Fig. 2B, C), the contrasts between loading values in the source space ($ARC1 > ARC2$ and $ARC2 > ARC1$) did not reach the significance level in this age group.

Given the location of ARC2 sources covering large territories in the temporal lobe, the analysis of its response to visual stimulation seemed to be essential for a more reliable attribution of ARC2 within the AR family. To this end, we used the phenomenon of "alpha-blocking" in response to eyes opening. Our analysis confirmed a significant attenuation of amplitude spectra of both ARC1 and ARC2 components in the REO versus REC condition, independent of age (Supplementary materials, Section III).

We found a 3-component structure only in 1 middle-aged participant (Fig. 1B). His alpha band included a single high-frequency component with predominantly occipito-parietal localization like ARC1 and 2 low-frequency occipito-temporal components ARC2 and ARC2' (akin to ARC2 in the 2-component AR). During the observation time, all the coexisting ARCs in the 2- and 3-component AR demonstrated individual behavior on a "seconds-to-minutes" time scale.

The proportion of middle-aged and older participants with a single-component AR structure was equal to 31% (10 participants out of 32) (Fig. 1C, D). Apparently, this subgroup was not homogenous. In 4 cases (49–60 years of age, Fig. 1C), the AR peaked at 10.6–11.4 Hz and was broadly distributed over posterior cortices. A comparison of the PARAFAC spectral loadings of this component with the AR spectra (ASD, Fig. 1C) suggests that these 4 participants might have strongly overlapping rhythms with close peak frequencies that we cannot reliably decompose by this technique. Similar structure was found in the same proportion of young participants (Barzegaran et al., 2017). In the remaining 6 participants (58–71 years of age, Fig. 1D), the AR peak frequency was between 7.4 and 9.6 Hz, whereas its sources were predominantly occipito-temporal or temporal.

3.2. Stability of AR structure in middle-aged and older participants

All types of AR structure were relatively stable during a single recording session in all the participants on a "minutes-to-hours" time scale (Fig. 1A–D, the fourth row). The mean temporal loadings for ARC1 varied across REC periods between 0.42 and 0.48 and for ARC2, between 0.33 and 0.38. Among 8 participants with follow-up sessions, 6 participants had a multicomponent AR structure and 2 participants, a single ARC (Fig. 3). In all the participants, the frequency and spatial features of all the ARCs were stable over the 2 recordings ($TCC > 0.85$).

3.3. Evolution of AR structure over adult lifespan

We considered the characteristics of the typical 2-component AR structure for the whole sample of 20- to 81-year-old participants as a starting point for the analysis of age-related trends. At the group level (45 participants with the 2- or 3-component AR structure), the ARC1 had a mean peak frequency of 10.2 $\pm$ 0.7 Hz; its maximum was localized to BA37, and it was significantly stronger than ARC2 in the occipito-parietal regions of the neocortex, including dorsal and medial parts where 96% of sources localized to BA17-19, 7, 23. ARC2 had a peak frequency of 9.2 $\pm$ 0.8 Hz, its maximum loading in BA37 and dominated over ARC1 in the lateral and ventral temporal cortices, where 86% of sources located in BA20, 21, 38, 48, 11 (Fig. 4).

The linear regression analysis, performed on the same group of participants with multicomponent AR, showed that peak frequencies of both ARCs decreased with age, although this trend was stronger for ARC1, which changed by 0.025 Hz/y, while ARC2, by 0.016 Hz/y (Fig. 5A). Accordingly, the frequency overlap between the ARC peaks increased with age (Fig. 5B), although their width did not change significantly. The amplitude ratio of ARC1/ARC2 had a weak tendency to decrease (Fig. 5C). The regression of spatial loadings against age revealed the relative weakening of ARC1 in the occipito-parietal regions (BA17-19, Fig 5D) but did not show any significant changes of ARC2. Finally, the regression analysis showed that the coordinates of both ARC maxima in MNI space shifted with age anteriorly and inferiorly but not laterally (Fig. 5E–G).

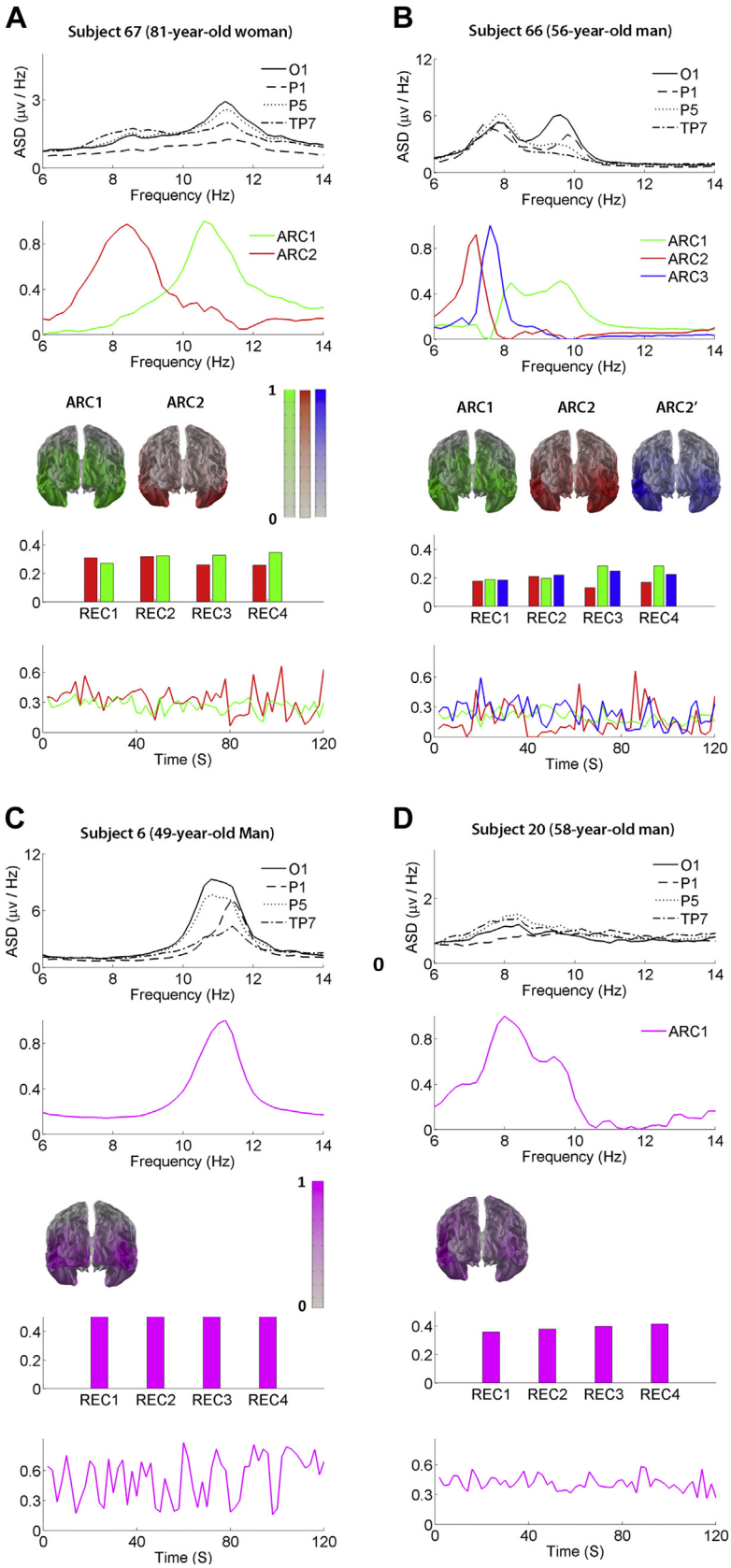

Fig. 1. Individual examples of 2-, 1-, and 3-component structure of AR. For each panel, A, B, C, and D, the first (upper) row shows the ASD of EEGs from posterior electrodes (O1, P1, P5, and TP7 according to the International 10/20 System) in the extended AR frequency range (the spectra in the conventional frequency range [1–45 Hz] for F3, F4, C3, C4, P3, P4, T7, T8, O1, and O2 are shown in Supplementary materials, Section IV). The second row shows the frequency loadings of ARCs; the third row shows the normalized source distributions of the ARCs (spatial loadings of the components) that are rendered on the average MNI brain (posterior view); the fourth and fifth rows show averages over the 4 REC periods and temporal loadings over representative 3-minute periods, respectively. Green lines, bars, and brain images refer to ARC1, red to ARC2, and blue to ARC2'. In the brain images, color indicates loading values: the higher the color intensity, the higher the loadings. The dimensionless loading values (y-axes in the second, fourth, and fifth rows) are normalized to the maximum value of each loading matrix. Abbreviations: AR, alpha rhythm; ARCs, AR components; ASD, amplitude spectrum densities; EEG, electroencephalogram; MNI, Montreal Neurological Institute; REC, resting state with eyes closed.

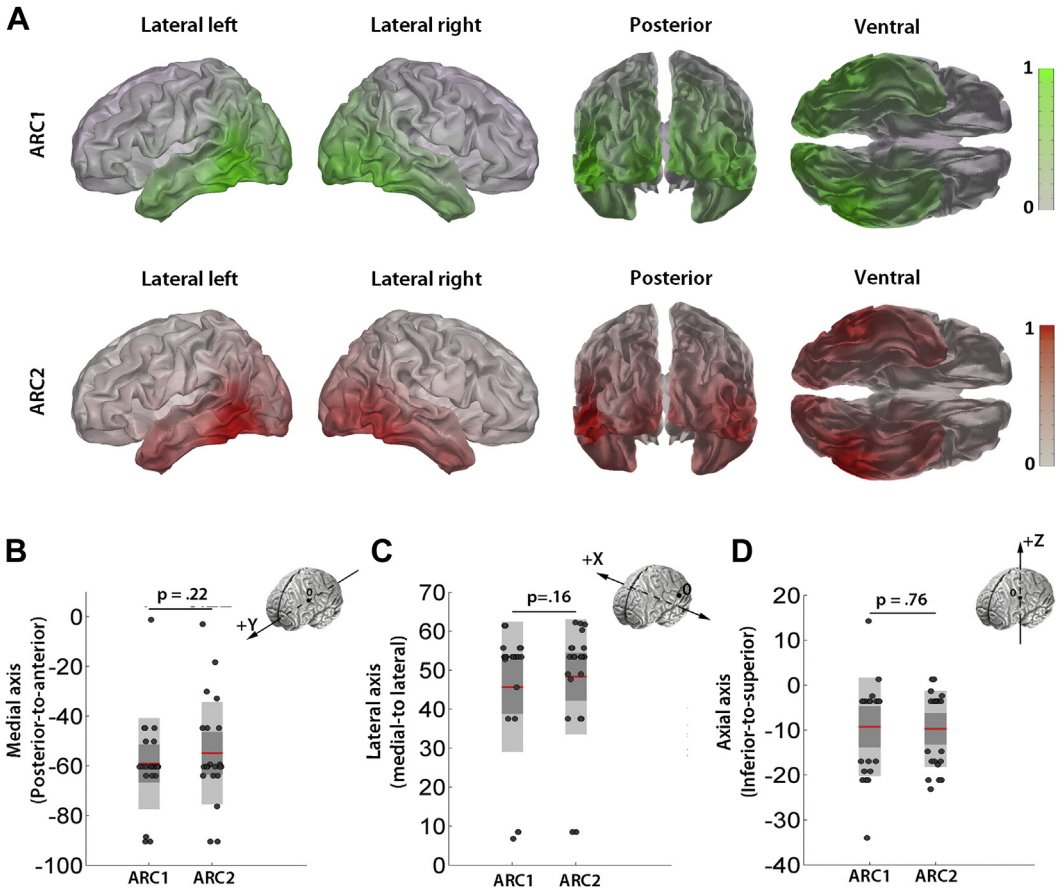

Fig. 2. Group-averaged cortical sources and individual maxima of ARC1 and ARC2 in middle-aged and older participants. In the panel A, the average normalized spatial loadings (the sum of loading vectors is set to 1) of ARC1 (in green) and ARC2 (in red) are shown for the sample of middle-aged and aged participants in the first and second rows, respectively. In panels B, C, and D, the box plots represent individual coordinates of ARC1 and ARC2 maxima. The red lines indicate the average, the dark gray boxes, the standard error of mean with 95% confidence interval, and the light gray boxes show 1 standard deviation. The raw data points are plotted on top of the box plots. At the top of each plot, *p*-value for paired *t*-test for the ARC1 versus ARC2 contrast is presented. Abbreviation: ARCs, AR components.

Although we found all types of AR structures (varying from 1 to 3 components) without a significant difference in their distribution between men and women ($p = 0.7$, Wilcoxon rank-sum test) across the entire adult lifespan, the relative proportions of these configurations changed with age (Fig. 6). Specifically, we showed the multicomponent structure in 89% of the young-age group. The dominant 2-component structure was encountered in 82% of young participants. In contrast, in the middle/old-age group, the multicomponent structure was limited to 69% and the 2-component structure, to 66% of participants, whereas the proportion of participants with a single-component AR structure attained 31% against 11% in the young group.

4. Discussion

4.1. Multicomponent structure of AR is lost with aging

Our analysis of neurologically healthy adults showed that the multicomponent structure of the AR is the rule, rather than the exception as previously suggested (Lodder and van Putten, 2011; Robinson et al., 2003). In young adults, at least 2 typical ARCs—high-frequency ARC1 and low-frequency ARC2—originating from occipito-parietal and occipito-temporal cortices, respectively—are likely to have partially different mechanisms of generation (for discussion see Barzegaran et al. (2017) and references therein). Multiple studies emphasized the phenomenological and functional heterogeneity of the AR (*ibid.*). However, despite a general agreement that the posterior AR is not a unitary phenomenon, the AR decomposition literature widely differs with respect to the number, topography, and functional attribution of the reported AR components.

In a study by Ramkumar et al. (2012), the authors applied a spatial Independent Component Analysis and spatial Fourier Independent Component Analysis to magnetoencephalography (MEG) data in cortical space. On average, they reported more than 10 components per participant in the 8–15 Hz band. While the authors localized the majority of them to the occipital lobe, in some participants they found AR components in the temporal lobe. Unfortunately, the low-frequency resolution of 1 Hz, which is not sufficient to estimate reliably the shape of the spectral peaks, did not allow the authors to classify systematically the components based on their spectra. The analysis did not impose any restrictions on the number of components, and therefore, their multiplicity could be an artificial result of "overfitting" the data.

In the context of aging, the following studies devoted to the analysis of the AR structure are of special interest. Chiang et al. (2011) analyzed REC EEGs from about 1500 normal 6- to 86-year-old participants by first, fitting individual power spectra by Gaussian peaks, and then, separating them into clusters defined by their frequency, spatial extent, and anterior-to-posterior position. The authors found 2 AR clusters, which closely resemble ARC1 and ARC2 of the present study, in 44% of participants regardless of their age. The relatively small proportion of participants with the 2 AR clusters can be explained by the limitations of the algorithm, which used the

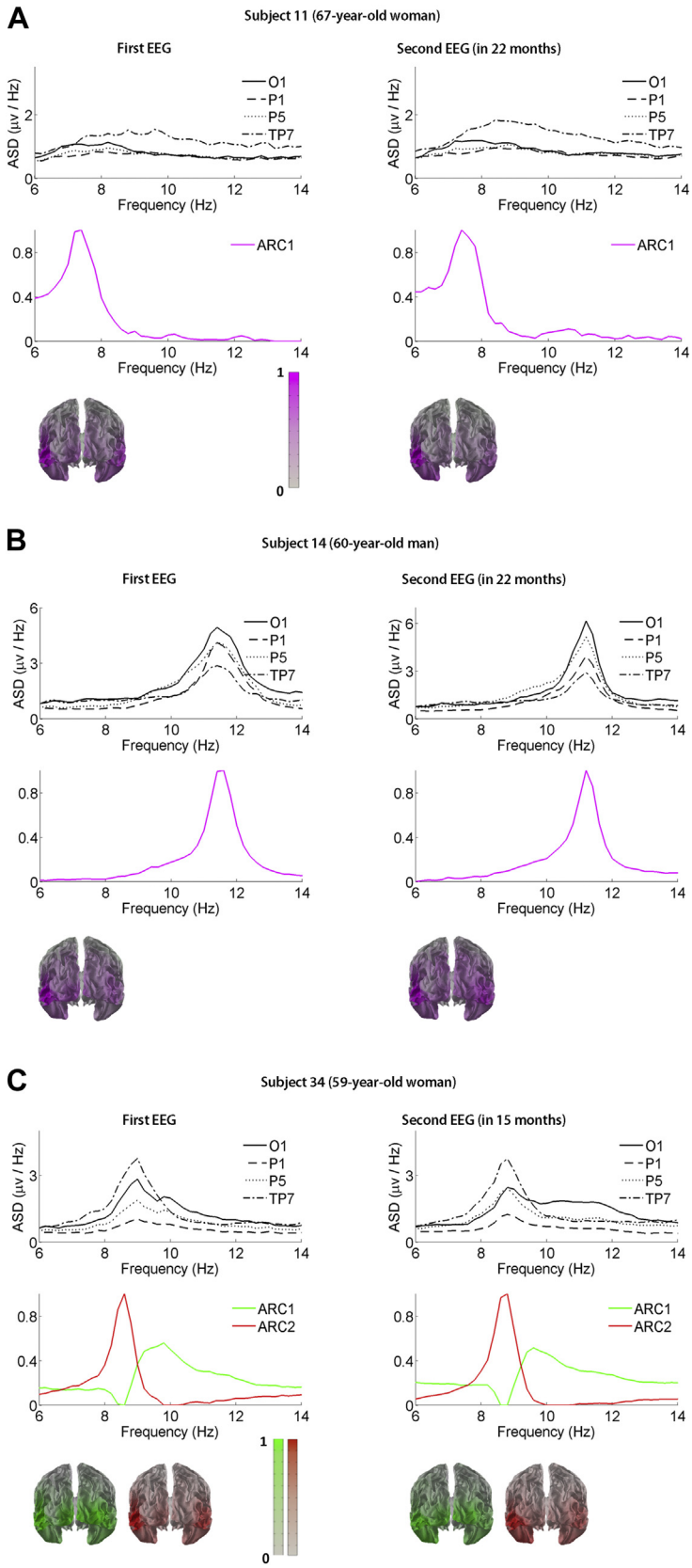

Fig. 3. Individually stable alpha structure with single and multiple components. The examples show 2 EEG recordings, separated by several months, of participants with single and multiple components of alpha. Abbreviations: ASD, amplitude spectrum densities; EEG, electroencephalogram. Other designations are as in Figure 1.

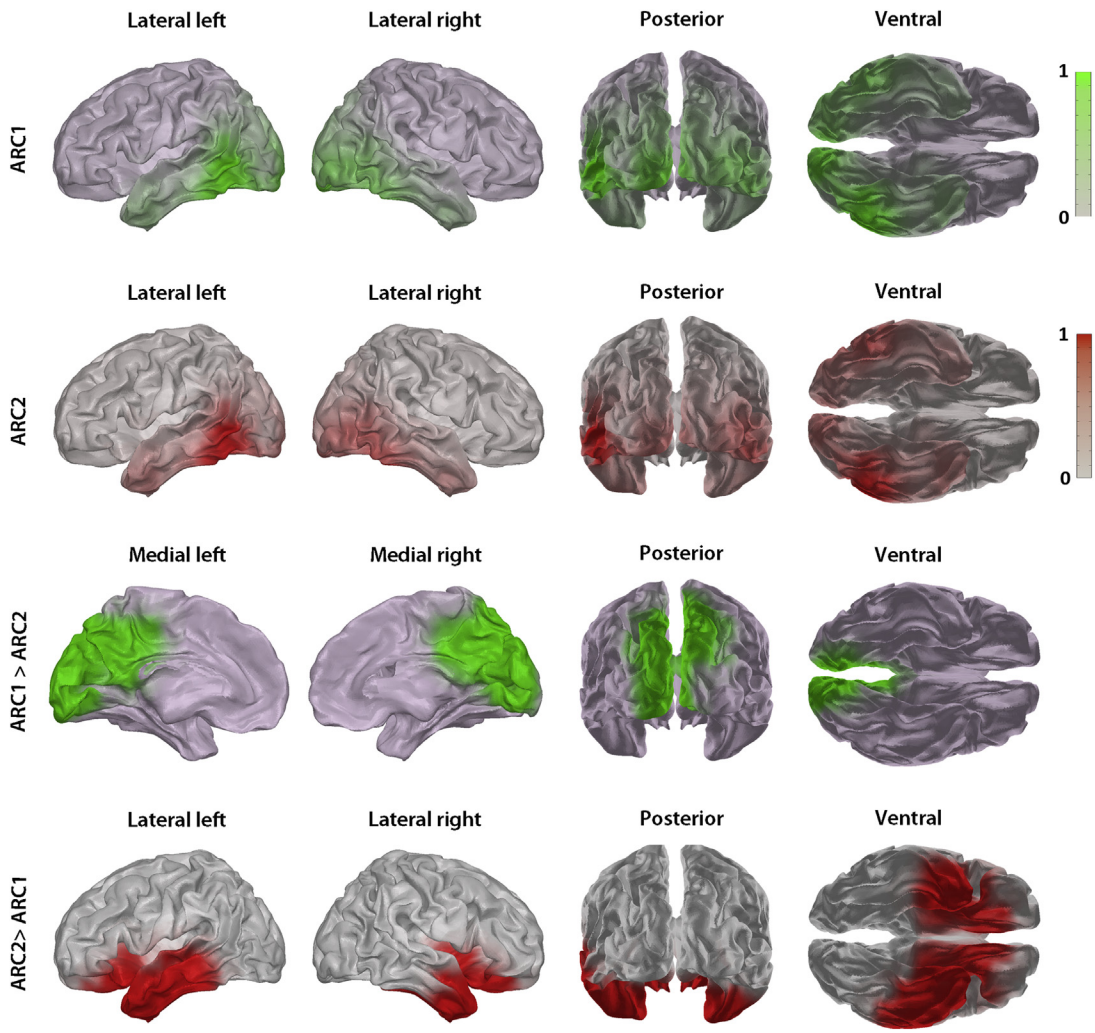

Fig. 4. Group-level spatial distributions and statistics of ARCs for all participants with 2-component AR structure. Group-averaged normalized spatial loadings (sum of loading vectors set to 1) of ARC1 and ARC2 are shown for the sample of forty-five 20- to 81-year-old participants in the first and second rows. On the third and fourth rows, we present the results of cluster-based statistics for comparing loading vectors of ARC1 and ARC2. ARC1 is significantly stronger in the occipito-parietal regions, whereas ARC2 dominates in the occipito-temporal or temporal regions. Abbreviations: AR, alpha rhythm; ARCs, AR components. Other designations are as in Figure 2.

frequency and space information, but discarded the temporal dimension of the data, thus limiting the resolution of the method.

Lodder and van Putten (2011) exploited a similar algorithm to estimate the amplitude and frequency characteristics of the posterior AR in a sample of 1089 normal EEGs from participants ranging from a few months to 96 years of age. Their choice of analyzing only 2 occipital derivations and a fitting algorithm that heavily penalized multicomponent solutions resulted in finding multiple peaks in only 1.6% participants and essentially reporting the age-dependent changes of a dominant ARC. Owing to the failure to separate individual components in many participants, neither of these studies showed the age-related evolution of the component structure of the AR.

In contrast, with the AR decomposition via PARAFAC, we found a stable multicomponent structure in 78% of normal adults between 20 and 81 years of age. Typically, it consisted of the 2 AR components, although we also encountered 3- and 1-component configurations. The proportion of participants with the single-component AR increased with age. The uneven occurrence of these AR configurations over the adult lifespan suggests a transformation of the multicomponent AR into a single-component AR with age. In the next sections, we consider how the accumulation of subtle changes in the individual characteristics of ARCs can lead to the gradual erosion of the AR structure and what neurobiological processes could be behind these changes.

4.2. Alpha-rhythm components: aging trends

The changes of the AR components over the adult lifespan can be reduced to the common trends, which, however, are implemented with different speeds of changes. Both components slow down over the adult lifespan, with the higher frequency component (ARC1) showing a more pronounced reduction of the peak frequency, which results in the increasing overlap of the components in the frequency domain. ARC1, which is occipito-parietal in early adulthood, becomes more distributed over the posterior association cortices with age, with its maximum moving from the dorsal midline territories of BA18/19 (Barzegaran et al., 2017) to BA37. Although the spatial loadings of the low-frequency component (ARC2), which represents oscillatory activities of the occipito-temporal region in young adults, do not correlate significantly with age, its maximum loading shifts anteriorly, while remaining within BA37. The amplitude ratio of ARC1 to ARC2 shows a

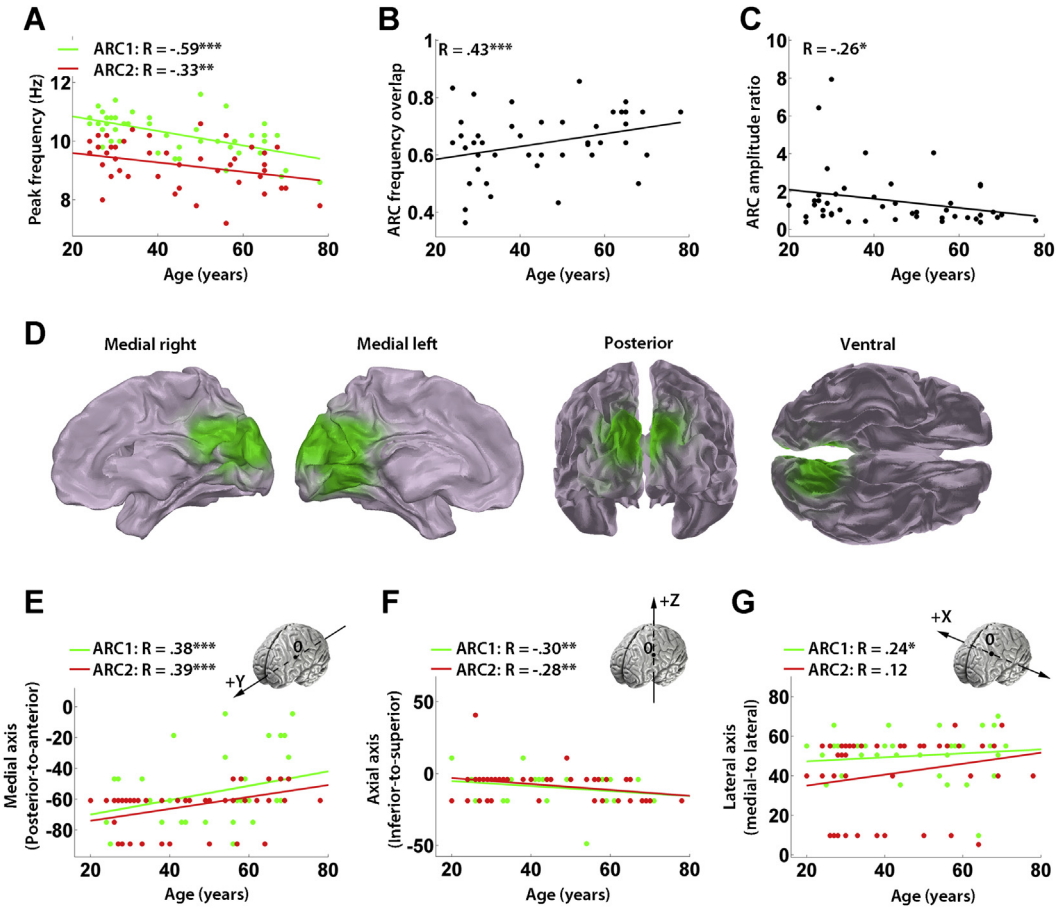

Fig. 5. Age trends for frequency and spatial features of ARCs. In the panels A, B, and C, we show scatter plots of the peak frequencies of ARC1 and ARC2, ARC frequency overlap and amplitude ratio and their regression with age. The plots in panel D represent the significant result of regression analysis of the normalized spatial loadings of ARC1 on age after cluster-based multiple comparison correction, rendered with green color on average MNI brain. In the panels E, F, and G, we present the scatter plots of the locations for sources with maximum spatial loadings and their regression lines on age are presented along the 3 axes of coordinates. In the panels A, B, C, E, F and G, the regression is presented with a solid line and the R statistics for the regression is shown, where * stands for $p < 0.1$, ** for $p < 0.05$, and *** for $p < 0.01$. Abbreviation: ARCs, AR components.

downward trend revealing the predominant loss of occipito-parietal activity in the AR frequency range.

4.3. Spatial rearrangement of AR components over adult lifespan

The relocation of ARC1 with age leads to its relative reduction in the cuneus and nearby cortices along the occipito-parietal midline and in the medial aspects of the hemispheres (Fig. 5). Similar descending tendency has been previously reported for the dominant posterior AR, an ARC1 proxy (Lodder and van Putten, 2011; Van Sweden et al., 1999; Vysata et al., 2012). This relative weakening of ARC1 sources in the utmost posterior regions might reflect the atrophy of the gray matter (GM) or match to the cortical areas that compensate for age-related changes and therefore maintain a higher level of activation associated with lower ARC1 loadings. In the first case, we would expect colocalization of this region with the areas that are the most vulnerable to neurodegeneration.

In normal adults in their seventies, the midline parietal and occipital regions show an annual GM loss of about 2%, whereas the average loss for the whole cortex is less than 1% (Thompson et al., 2003), suggesting connection of the ARC1 decline with the GM degeneration. However, in contrast to the precuneus, lateral parietal and temporal association cortices, and the posterior cingulate, where GM atrophy, hypometabolism, and amyloid plaque deposition are consistently found in many clinically normal older adults (Buckner et al., 2009; Jack et al., 2008; Rabinovici et al., 2010; Reiman, 2007; Villemagne et al., 2011), the cuneus seems to be relatively spared. Moreover, the GM atrophy rates are, probably, much lower for younger adults, who constitute most of our sample.

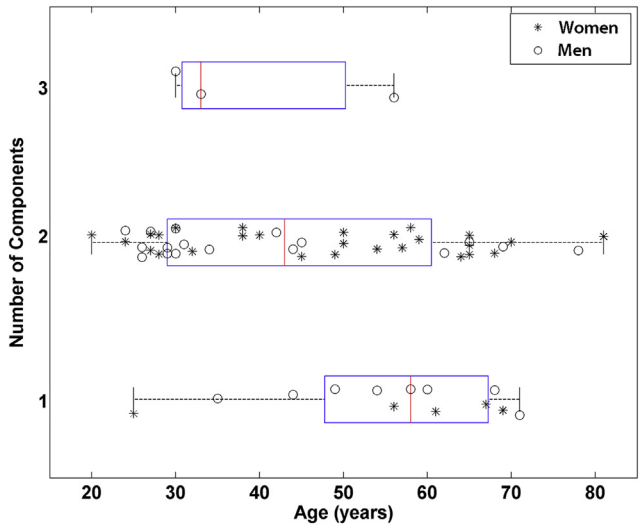

Fig. 6. Distribution of the 1-, 2-, and 3-component structures of AR in adults of different ages and genders. The red lines represent the median and boxes represent the 25th and 75th percentiles of age for the participants with a particular AR structure. Abbreviation: AR, alpha rhythm.

These considerations work in favor of the assumption that the relative weakening of ARC1 in normal aging is a byproduct of decreasing activation and metabolism in the posterior association areas surrounding the cuneus or linked to compensatory strategies implemented by cuneal networks—assumptions that do not conflict with each other. Indeed, in the older adults, the cuneus has been shown to function as a neural reserve, that is, to be an alternative to the regions typically used by younger adults (Cabeza, 2001; Tucker and Stern, 2011). In this context, we can consider the relative reduction of ARC1 amplitude loadings as a sign of additional activation due to remapping of the cuneus and nearby territories. The decreased AR index found with advancing age (Van Sweden et al., 1999) also supports this assumption.

Considering the pronounced GM loss in older adults in the posterior temporal association areas, we might expect to find an inverse correlation of ARC2 amplitude loadings with age. However, this was not the case. Matching observations have been reported in an early longitudinal study, which showed predominant decline of the high-frequency AR in healthy participants during their 7th decade of life (Wang and Busse, 1969). A plausible explanation seems to be an increasing overlap between ARC1 and ARC2, which finally leads to the fusion of both components at the low-frequency AR range, masking the changes of ARC2 per se. Another reason could be the minor-only GM changes in the sample of young and middle-aged healthy controls.

Indeed, a correlation between the amplitude of the predefined low-frequency AR, a proxy of ARC2, and the average occipital GM density found in a mixed group of aged normal participants and patients with mild cognitive impairment (MCI), or Alzheimer's disease (AD), suggests that it is due to the GM variability on a major scale (Babiloni et al., 2015). On the other hand, the fading of the high-frequency component with age and its further decline in MCI/AD patients (Garcés et al., 2013; Knyazeva et al., 2010; Prichep, 2007) could prevent significant findings for the high-frequency AR in Babiloni et al.'s study of older adults, owing to decreasing signal-to-noise ratio. Then, aggregating the results from both reports, we can infer that the earliest signs of age-related changes are ARC1 diminishing in the middle age population, followed by ARC2 declining in MCI/AD.

The apparent "moving" of the AR sources with age and even more so with progressing neurodegeneration in the MCI-AD sequence was reported previously (Babiloni et al., 2016; Huang et al., 2000; Prichep, 2007). The anteriorization of the occipito-temporal ARC2 raises the question of the relationship between this component and the "third" or "tau" rhythm (Niedermeyer, 1993). In contrast to MEG studies (Lehtelä et al., 1997; Tiihonen et al., 1991) that reported the tau rhythm as spontaneous 8–10 Hz activity affected by auditory but not visual stimuli, in EEG recordings, the tau rhythm was thought for a long time to be a hidden phenomenon. Specifically, the 6- to 9-Hz rhythm localized to the temporal region could be detected either by means of electrocorticography or by surface EEG from patients with a bone defect over the temporal lobe ("breach rhythm"), but not in young healthy controls (Cobb et al., 1979; Niedermeyer, 1990, 1997).

Conversely, in aged people, the alphoid rhythm can be easily recorded from temporal EEG electrodes in the resting state (Asokan et al., 1987). Niedermeyer (1997) wondered whether this rhythm is identical to the "breach rhythm," and what is a mechanism that renders it visible on the surface EEG of older people. According to our analysis of the reactivity of both components (Supplementary materials, Section III), both occipito-parietal ARC1 and occipito-temporal ARC2 respond to eyes opening with statistically significant attenuation, irrespectively of age. Therefore, we can consider ARC2, which "moves" with age in the anterior direction, as a component of the posterior (visual) AR. Then, the anteriorization of ARC2 sources, shown here, and the emergence of the slow AR in older people, described in the literature, seem to represent different aspects of the same phenomenon.

4.4. AR slowing in the context of multicomponent structure

Although the literature frequently mentions the AR slowing with age, statistical analyses do not always support this observation. The effect is obvious in the oldest old, in whom the alpha peak frequency is about 8–8.5 Hz (Hubbard et al., 1976; Peltz et al., 2010), while in the middle-aged and older participants, many authors failed to find it (Caplan et al., 2015; Duffy et al., 1993; Gaál et al., 2010; Pollock et al., 1990). According to our data, the process is indeed very slow, at least in neurologically normal participants, and its detection requires relatively high-frequency resolution, which was not the case in many studies. Importantly, in our sample, we found direct correlations between ARC1 peak frequency and the performance of the letter fluency test and MoCA (Supplementary materials, Section V). Significant difference in the mean frequency of the posterior AR was also found between normal older adults, who declined in the MCI and AD over the next 7 years and those with stable cognitive abilities, within this period (Prichep et al., 2006). Therefore, the ARC1 peak frequency is an important neurobiological index of cognitive aging.

We found that the AR slowing is a complex process that involves slowing and weakening of both components (more expressed for the high-frequency ARC1) and their fusion at low frequencies. Our estimation of this trend is quite conservative because only participants with preserved 2-component structure were included in the regression analysis. Potential mechanisms of slowing should be able to explain both common trends and the differences between ARC1 and ARC2. Considering the thalamo-cortical mechanisms of the AR generation (Buzsaki, 2006; Hughes and Crunelli, 2005; Niedermeyer, 1997), the thalamic lesions putatively impact to the common constituent of the frequency changes of ARC1 and ARC2 (Mäkelä et al., 1998), while their differences can be ascribed to the aging of cortico-cortical association fibers.

Reports concerning the AR links to the white matter mainly considered the parameters of the occipito-parietal AR, that is, virtually, ARC1, which dominates in young adults (Barzegaran et al., 2017). A recent study, based on a combination of MEG, diffusion tensor imaging, and biophysical modeling, showed that the source AR amplitudes throughout the visual cortex could be well predicted by the propagation of oscillations from the primary visual cortex via cortico-cortical pathways, both in dorsal (occipito-parietal) and ventral (occipito-temporal) streams (Hindriks et al., 2015). The predictive power of the model was high over the territories extending in 1 direction from the occipital to parietal lobe, and, in another direction, from the occipital to the temporal lobe in line with the localization of ARC1 and ARC2, respectively.

The connections between the occipital and parietal lobes are carried out over superior longitudinal fasciculus (SLF), while the connections between the occipital and temporal lobes are carried out via the inferior longitudinal fasciculus (ILF), both pathways being duplicated by U-fibers (Catani et al., 2003; De Schotten et al., 2011; Ffytche et al., 2010). Starting with the 5th decade of age, the cerebral white matter undergoes uneven changes: the association fibers seem to decline faster than the commissural or projection fibers (Bender et al., 2016; Cox et al., 2016; Sexton et al., 2014; Sullivan et al., 2010; Yeatman et al., 2014; de Groot et al., 2015). Among association tracts, the ILF and SLF display considerable age-related decline (Bosch et al., 2012; Tian et al., 2016; Yeatman et al., 2014), and their demyelination inversely correlates with episodic memory performance (Carmeli et al., 2013).

The functions that suffer from ILF pathology belong to the ventral processing stream (face and object recognition, etc.), and those that are compromised by the SLF impairment are related to the dorsal stream (spatial orientation, attention, etc.) (ffytche et al., 2010; Ortibus et al., 2012). Importantly, older individuals show visual stream–specific deficits including a more gradual decline of form-related than motion- and space-related cognitive functions (Hutchinson et al., 2012; Moffat, 2009; Porter et al., 2017). Based on our hypothesis that the ARC1 is inherent in the dorsal visual stream, while ARC2, in the ventral visual stream (Barzegaran et al., 2017), it would be extremely enlightening to integrate the evidence on the aging of ARC1 and ARC2 with the data on the aging of SLF and ILF, respectively. However, to the best of our knowledge, no one has yet reported this information.

4.5. Conclusion and methodological implications

We expect that detailed knowledge of the component structure of the AR and its age-related changes will be useful for monitoring aging and neurodegenerative processes in the human brain. A common approach of subdividing the EEG spectrum in the alpha range into the low- and high-frequency AR with predefined borders seems misleading because the inherent component structure of the AR can be misrepresented by such an arbitrary segmentation. The use of individual alpha frequency as a boundary between the AR sub-bands (e.g., in Zappasodi et al. (2015)) cannot be recommended because the same (dominant!) ARC would be shared between both sub-bands with the exception of rare cases of 2 components with equal amplitudes. The accurate segmentation of the AR is especially important for developmental and aging research because characteristic frequencies and even the component structure of the AR per se change over the lifespan. Data-driven analysis of the inherent component structure should precede the investigation of the AR functionality or pathological changes. To this end, we can recommend PARAFAC as a decomposition technique that uses the full extent of time, space, and frequency dimensions of EEG and successfully separates the AR into its components in most individuals.

Acknowledgements

This work was supported by Swiss Research Program Nano-Tera (BodyPoweredSenSE project) grant to Maria G. Knyazeva. The authors wish to thank Ms. Melanie Price Hirt for assistance in the preparation of the article and all the participants for their willingness to contribute time and effort to this study.

Disclosure statement

The authors have no actual or potential conflicts of interest.

Appendix A. Supplementary data

Supplementary data associated with this article can be found, in the online version, at https://doi.org/10.1016/j.neurobiolaging.2018.05.018.

References

Andersson, C.A., Bro, R., 2000. The N-way toolbox for MATLAB. Chemometr. Intell. Lab. Syst. 52, 1–4.
Angelakis, E., Stathopoulou, S., Frymiare, J.L., Green, D.L., Lubar, J.F., Kounios, J., 2007. EEG neurofeedback: a brief overview and an example of peak alpha frequency training for cognitive enhancement in the elderly. Clin. Neuropsychol. 21, 110–129.
Asokan, G., Pareja, J., Niedermeyer, E., 1987. Temporal minor slow and sharp EEG activity and cerebrovascular disorder. Clin. Electroencephalogr. 18, 201–210.
Babiloni, C., Binetti, G., Cassarino, A., Dal Forno, G., Del Percio, C., Ferreri, F., Ferri, R., Frisoni, G., Galderisi, S., Hirata, K., 2006. Sources of cortical rhythms in adults during physiological aging: a multicentric EEG study. Hum. Brain Mapp. 27, 162–172.
Babiloni, C., Del Percio, C., Boccardi, M., Lizio, R., Lopez, S., Carducci, F., Marzano, N., Soricelli, A., Ferri, R., Triggiani, A.I., 2015. Occipital sources of resting-state alpha rhythms are related to local gray matter density in subjects with amnesic mild cognitive impairment and Alzheimer's disease. Neurobiol. Aging 36, 556–570.
Babiloni, C., Del Percio, C., Caroli, A., Salvatore, E., Nicolai, E., Marzano, N., Lizio, R., Cavedo, E., Landau, S., Chen, K., 2016. Cortical sources of resting state EEG rhythms are related to brain hypometabolism in subjects with Alzheimer's disease: an EEG-PET study. Neurobiol. Aging 48, 122–134.
Barzegaran, E., Vildavski, V.Y., Knyazeva, M.G., 2017. Fine structure of posterior alpha rhythm in human EEG: frequency components, their cortical sources, and temporal behavior. Sci. Rep. 7, 8249.
Başar, E., 2012. A review of alpha activity in integrative brain function: fundamental physiology, sensory coding, cognition and pathology. Int. J. Psychophysiol. 86, 1–24.
Bender, A.R., Völkle, M.C., Raz, N., 2016. Differential aging of cerebral white matter in middle-aged and older adults: a seven-year follow-up. Neuroimage 125, 74–83.
Bosch, B., Arenaza-Urquijo, E.M., Rami, L., Sala-Llonch, R., Junqué, C., Solé-Padullés, C., Peña-Gómez, C., Bargalló, N., Molinuevo, J.L., Bartrés-Faz, D., 2012. Multiple DTI index analysis in normal aging, amnestic MCI and AD. Relationship with neuropsychological performance. Neurobiol. Aging 33, 61–74.
Bro, R., 1997. PARAFAC. Tutorial and applications. Chemometr. Intell. Lab. Syst. 38, 149–171.
Bro, R., Kiers, H.A., 2003. A new efficient method for determining the number of components in PARAFAC models. J. Chemom. 17, 274–286.
Buckner, R.L., Sepulcre, J., Talukdar, T., Krienen, F.M., Liu, H., Hedden, T., Andrews-Hanna, J.R., Sperling, R.A., Johnson, K.A., 2009. Cortical hubs revealed by intrinsic functional connectivity: mapping, assessment of stability, and relation to Alzheimer's disease. J. Neurosci. 29, 1860–1873.
Buzsaki, G., 2006. Rhythms of the Brain. Oxford University Press, New York, NY, pp. 175–186.
Cabeza, R., 2001. Cognitive neuroscience of aging: contributions of functional neuroimaging. Scand. J. Psychol. 42, 277–286.
Caplan, J.B., Bottomley, M., Kang, P., Dixon, R.A., 2015. Distinguishing rhythmic from non-rhythmic brain activity during rest in healthy neurocognitive aging. Neuroimage 112, 341–352.
Carmeli, C., Donati, A., Antille, V., Viceic, D., Ghika, J., von Gunten, A., Clarke, S., Meuli, R., Frackowiak, R.S., Knyazeva, M.G., 2013. Demyelination in mild cognitive impairment suggests progression path to Alzheimer's disease. PLoS One 8, e72759.
Carroll, J.D., Chang, J.-J., 1970. Analysis of individual differences in multidimensional scaling via an N-way generalization of "Eckart-Young" decomposition. Psychometrika 35, 283–319.
Catani, M., Jones, D.K., Donato, R., Ffytche, D.H., 2003. Occipito-temporal connections in the human brain. Brain 126, 2093–2107.
Chiang, A., Rennie, C., Robinson, P., Van Albada, S., Kerr, C., 2011. Age trends and sex differences of alpha rhythms including split alpha peaks. Clin. Neurophysiol. 122, 1505–1517.
Clark, C.R., Veltmeyer, M.D., Hamilton, R.J., Simms, E., Paul, R., Hermens, D., Gordon, E., 2004. Spontaneous alpha peak frequency predicts working memory performance across the age span. Int. J. Psychophysiol. 53, 1–9.
Cobb, W., Guiloff, R., Cast, J., 1979. Breach rhythm: the EEG related to skull defects. Electroencephalogr. Clin. Neurophysiol. 47, 251–271.
Cox, S.R., Ritchie, S.J., Tucker-Drob, E.M., Liewald, D.C., Hagenaars, S.P., Davies, G., Wardlaw, J.M., Gale, C.R., Bastin, M.E., Deary, I.J., 2016. Ageing and brain white matter structure in 3513 UK Biobank participants. Nat. Commun. 7, 13629.
Davidson, P.N., Davidson, K.A., 2012. Electroencephalography in the elderly. Neurodiagnostic J. 52, 3–19.
de Groot, M., Ikram, M.A., Akoudad, S., Krestin, G.P., Hofman, A., van der Lugt, A., Niessen, W.J., Vernooij, M.W., 2015. Tract-specific white matter degeneration in aging: the Rotterdam Study. Alzheimers Dement 11, 321–330.
De Schotten, M.T., Dell'Acqua, F., Forkel, S.J., Simmons, A., Vergani, F., Murphy, D.G., Catani, M., 2011. A lateralized brain network for visuospatial attention. Nat. Neurosci. 14, 1245–1246.
Duffy, F.H., McAnulty, G.B., Albert, M.S., 1993. The pattern of age-related differences in electrophysiological activity of healthy males and females. Neurobiol. Aging 14, 73–84.
Ffytche, D.H., Blom, J.D., Catani, M., 2010. Disorders of visual perception. J. Neurol. Neurosurg. Psychiatry 81, 1280–1287.
Field, A.S., Graupe, D., 1991. Topographic component (parallel factor) analysis of multichannel evoked potentials: practical issues in trilinear spatiotemporal decomposition. Brain Topography 3, 407–423.
Fonov, V.S., Evans, A.C., McKinstry, R.C., Almli, C., Collins, D., 2009. Unbiased nonlinear average age-appropriate brain templates from birth to adulthood. Neuroimage 47, S102.
Fotenos, A.F., Snyder, A., Girton, L., Morris, J., Buckner, R., 2005. Normative estimates of cross-sectional and longitudinal brain volume decline in aging and AD. Neurology 64, 1032–1039.

Gaál, Z.A., Boha, R., Stam, C.J., Molnár, M., 2010. Age-dependent features of EEG-reactivity—spectral, complexity, and network characteristics. Neurosci. Lett. 479, 79–84.
Garcés, P., Vicente, R., Wibral, M., Pineda-Pardo, J.Á., López, M.E., Aurtenetxe, S., Marcos, A., de Andrés, M.E., Yus, M., Sancho, M., 2013. Brain-wide slowing of spontaneous alpha rhythms in mild cognitive impairment. Front. Aging Neurosci. 5, 100.
Ge, Y., Grossman, R.I., Babb, J.S., Rabin, M.L., Mannon, L.J., Kolson, D.L., 2002. Age-related total gray matter and white matter changes in normal adult brain. Part I: volumetric MR imaging analysis. AJNR. Am. J. Neuroradiol. 23, 1327–1333.
Harrison, T.M., Weintraub, S., Mesulam, M.-M., Rogalski, E., 2012. Superior memory and higher cortical volumes in unusually successful cognitive aging. J. Int. Neuropsychol. Soc. 18, 1081–1085.
Harshman, R.A., 1970. Foundations of the PARAFAC procedure: models and conditions for an "explanatory" multi-modal factor analysis. UCLA Working Papers in Phonetics 16, 1–84.
Hindriks, R., Woolrich, M., Luckhoo, H., Joensson, M., Mohseni, H., Kringelbach, M.L., Deco, G., 2015. Role of white-matter pathways in coordinating alpha oscillations in resting visual cortex. Neuroimage 106, 328–339.
Hong, X., Sun, J., Bengson, J.J., Mangun, G.R., Tong, S., 2015. Normal aging selectively diminishes alpha lateralization in visual spatial attention. Neuroimage 106, 353–363.
Huang, C., Wahlund, L.-O., Dierks, T., Julin, P., Winblad, B., Jelic, V., 2000. Discrimination of Alzheimer's disease and mild cognitive impairment by equivalent EEG sources: a cross-sectional and longitudinal study. Clin. Neurophysiol. 111, 1961–1967.
Hubbard, O., Sunde, D., Goldensohn, E.S., 1976. The EEG in centenarians. Electroencephalogr. Clin. Neurophysiol. 40, 407–417.
Hughes, S.W., Crunelli, V., 2005. Thalamic mechanisms of EEG alpha rhythms and their pathological implications. Neuroscientist. 11, 357–372.
Hutchinson, C.V., Arena, A., Allen, H.A., Ledgeway, T., 2012. Psychophysical correlates of global motion processing in the aging visual system: a critical review. Neurosci. Biobehav. Rev. 36, 1266–1272.
Jack Jr., C.R., Lowe, V.J., Senjem, M.L., Weigand, S.D., Kemp, B.J., Shiung, M.M., Knopman, D.S., Boeve, B.F., Klunk, W.E., Mathis, C.A., 2008. 11C PiB and structural MRI provide complementary information in imaging of Alzheimer's disease and amnestic mild cognitive impairment. Brain 131, 665–680.
Klimesch, W., 1999. EEG alpha and theta oscillations reflect cognitive and memory performance: a review and analysis. Brain Res. Rev. 29, 169–195.
Knyazeva, M.G., Jalili, M., Brioschi, A., Bourquin, I., Fornari, E., Hasler, M., Meuli, R., Maeder, P., Ghika, J., 2010. Topography of EEG multivariate phase synchronization in early Alzheimer's disease. Neurobiol. Aging 31, 1132–1144.
Launer, L., 2005. The epidemiologic study of dementia: a life-long quest? Neurobiol. Aging 26, 335–340.
Lawton, M.P., Brody, E.M., 1969. Assessment of older people: self-maintaining and instrumental activities of daily living. Gerontologist 9, 179–186.
Lehtelä, L., Salmelin, R., Hari, R., 1997. Evidence for reactive magnetic 10-Hz rhythm in the human auditory cortex. Neurosci. Lett. 222, 111–114.
Lockhart, S.N., DeCarli, C., 2014. Structural imaging measures of brain aging. Neuropsychol. Rev. 24, 271–289.
Lodder, S.S., van Putten, M.J., 2011. Automated EEG analysis: characterizing the posterior dominant rhythm. J. Neurosci. Methods 200, 86–93.
Lorenzo-Seva, U., Ten Berge, J.M., 2006. Tucker's congruence coefficient as a meaningful index of factor similarity. Methodology 2, 57–64.
Mäkelä, J.P., Salmelin, R., Kotila, M., Salonen, O., Laaksonen, R., Hokkanen, L., Hari, R., 1998. Modification of neuromagnetic cortical signals by thalamic infarctions. Electroencephalogr. Clin. Neurophysiol. 106, 433–443.
Maris, E., Oostenveld, R., 2007. Nonparametric statistical testing of EEG-and MEG-data. J. Neurosci. Methods 164, 177–190.
Markand, O.N., 1986. Electroencephalogram in dementia. Am. J. EEG Technol. 26, 3–17.
Moffat, S.D., 2009. Aging and spatial navigation: what do we know and where do we go? Neuropsychol. Rev. 19, 478.
Moretti, D.V., Babiloni, C., Binetti, G., Cassetta, E., Dal Forno, G., Ferreric, F., Ferri, R., Lanuzza, B., Miniussi, C., Nobili, F., 2004. Individual analysis of EEG frequency and band power in mild Alzheimer's disease. Clin. Neurophysiol. 115, 299–308.
Moretti, D., Prestia, A., Fracassi, C., Geroldi, C., Binetti, G., Rossini, P.M., Zanetti, O., Frisoni, G., 2011. Volumetric differences in mapped hippocampal regions correlate with increase of high alpha rhythm in Alzheimer's disease. Int. J. Alzheimers Dis. 2011, 208218.
Niedermeyer, E., 1990. Alpha-like rhythmical activity of the temporal lobe. Clin. Electroencephalogr. 21, 210–224.
Niedermeyer, E., 1993. The "third rhythm": alpha-like activity over the midtemporal region. Am. J. EEG Technol. 33, 159–173.
Niedermeyer, E., 1997. Alpha rhythms as physiological and abnormal phenomena. Int. J. Psychophysiol. 26, 31–49.
Ortibus, E., Verhoeven, J., Sunaert, S., Casteels, I., De Cock, P., Lagae, L., 2012. Integrity of the inferior longitudinal fasciculus and impaired object recognition in children: a diffusion tensor imaging study. Dev. Med. Child Neurol. 54, 38–43.
Pascual-Marqui, R.D., Michel, C.M., Lehmann, D., 1994. Low resolution electromagnetic tomography: a new method for localizing electrical activity in the brain. Int. J. Psychophysiol. 18, 49–65.
Peltz, C.B., Kim, H.L., Kawas, C.H., 2010. Abnormal EEGs in cognitively and physically healthy oldest-old: findings from the 90+ study. J. Clin. Neurophysiol. 27, 292–295.
Pfefferbaum, A., Rohlfing, T., Rosenbloom, M.J., Chu, W., Colrain, I.M., Sullivan, E.V., 2013. Variation in longitudinal trajectories of regional brain volumes of healthy men and women (ages 10 to 85 years) measured with atlas-based parcellation of MRI. Neuroimage 65, 176–193.
Pollock, V., Schneider, L., Lyness, S., 1990. EEG amplitudes in healthy, late-middle-aged and elderly adults: normality of the distributions and correlations with age. Electroencephalogr. Clin. Neurophysiol. 75, 276–288.
Porter, G., Wattam-Bell, J., Bayer, A., Haworth, J., Braddick, O., Atkinson, J., Tales, A., 2017. Different trajectories of decline for global form and global motion processing in aging, mild cognitive impairment and Alzheimer's disease. Neurobiol. Aging 56, 17–24.
Prichep, L.S., 2007. Quantitative EEG and electromagnetic brain imaging in aging and in the evolution of dementia. Ann. N Y Acad. Sci. 1097, 156–167.
Prichep, L., John, E., Ferris, S., Rausch, L., Fang, Z., Cancro, R., Torossian, C., Reisberg, B., 2006. Prediction of longitudinal cognitive decline in normal elderly with subjective complaints using electrophysiological imaging. Neurobiol. Aging 27, 471–481.
Rabinovici, G.D., Furst, A.J., Alkalay, A., Racine, C.A., O'neil, J.P., Janabi, M., Baker, S.L., Agarwal, N., Bonasera, S.J., Mormino, E.C., 2010. Increased metabolic vulnerability in early-onset Alzheimer's disease is not related to amyloid burden. Brain 133, 512–528.
Ramkumar, P., Parkkonen, L., Hari, R., Hyvärinen, A., 2012. Characterization of neuromagnetic brain rhythms over time scales of minutes using spatial independent component analysis. Hum. Brain Mapp. 33, 1648–1662.
Raz, N., Lindenberger, U., Rodrigue, K.M., Kennedy, K.M., Head, D., Williamson, A., Dahle, C., Gerstorf, D., Acker, J.D., 2005. Regional brain changes in aging healthy adults: general trends, individual differences and modifiers. Cereb. Cortex. 15, 1676–1689.
Reiman, E.M., 2007. Linking brain imaging and genomics in the study of Alzheimer's disease and aging. Ann. N Y Acad. Sci. 1097, 94–113.
Rickham, P.P., 1964. Human experimentation: code of ethics of the World Medical Association. Declaration of Helsinki. Br. Med. J. 2, 177–177.
Robinson, P., Whitehouse, R., Rennie, C., 2003. Nonuniform corticothalamic continuum model of electroencephalographic spectra with application to split-alpha peaks. Phys. Rev. E Stat. Nonlin. Soft Matter Phys. 68, 021922.
Rogalski, E., Gefen, T., Mao, Q., Connelly, M., Weintraub, S., Geula, C., Bigio, E.H., Mesulam, M.M., 2018. Cognitive trajectories and spectrum of neuropathology in Super Agers: the first 10 cases. Hippocampus. https://doi.org/10.1002/hipo.22828 [Epub ahead of print].
Rogalski, E.J., Gefen, T., Shi, J., Samimi, M., Bigio, E., Weintraub, S., Geula, C., Mesulam, M.M., 2013. Youthful memory capacity in old brains: anatomic and genetic clues from the Northwestern SuperAging Project. J. Cogn. Neurosci. 25, 29–36.
Rossini, P., Del Percio, C., Pasqualetti, P., Cassetta, E., Binetti, G., Dal Forno, G., Ferreri, F., Frisoni, G., Chiovenda, P., Miniussi, C., 2006. Conversion from mild cognitive impairment to Alzheimer's disease is predicted by sources and coherence of brain electroencephalography rhythms. Neuroscience 143, 793–803.
Salthouse, T.A., 2009. When does age-related cognitive decline begin? Neurobiol. Aging 30, 507–514.
Sexton, C.E., Walhovd, K.B., Storsve, A.B., Tamnes, C.K., Westlye, L.T., Johansen-Berg, H., Fjell, A.M., 2014. Accelerated changes in white matter microstructure during aging: a longitudinal diffusion tensor imaging study. J. Neurosci. 34, 15425–15436.
Shigeta, M., Julin, P., Almkvist, O., Basun, H., Rudberg, U., Wahlund, L.-O., 1995. EEG in successful aging; a 5 year follow-up study from the eighth to ninth decade of life. Electroencephalogr. Clin. Neurophysiol. 95, 77–83.
Singh-Manoux, A., Kivimaki, M., Glymour, M.M., Elbaz, A., Berr, C., Ebmeier, K.P., Ferrie, J.E., Dugravot, A., 2012. Timing of onset of cognitive decline: results from Whitehall II prospective cohort study. BMJ 344, d7622.
Sullivan, E.V., Rohlfing, T., Pfefferbaum, A., 2010. Quantitative fiber tracking of lateral and interhemispheric white matter systems in normal aging: relations to timed performance. Neurobiol. Aging 31, 464–481.
Thompson, P.M., Hayashi, K.M., De Zubicaray, G., Janke, A.L., Rose, S.E., Semple, J., Herman, D., Hong, M.S., Dittmer, S.S., Doddrell, D.M., 2003. Dynamics of gray matter loss in Alzheimer's disease. J. Neurosci. 23, 994–1005.
Tian, Q., Ferrucci, L., Resnick, S.M., Simonsick, E.M., Shardell, M.D., Landman, B.A., Venkatraman, V.K., Gonzalez, C.E., Studenski, S.A., 2016. The effect of age and microstructural white matter integrity on lap time variation and fast-paced walking speed. Brain Imaging Behav. 10, 697–706.
Tiihonen, J., Hari, R., Kajola, M., Karhu, J., Ahlfors, S., Tissari, S., 1991. Magnetoencephalographic 10-Hz rhythm from the human auditory cortex. Neurosci. Lett. 129, 303–305.
Tucker, A.M., Stern, Y., 2011. Cognitive reserve in aging. Curr. Alzheimer Res. 8, 354–360.
Vaden, R.J., Hutcheson, N.L., McCollum, L.A., Kentros, J., Visscher, K.M., 2012. Older adults, unlike younger adults, do not modulate alpha power to suppress irrelevant information. Neuroimage 63, 1127–1133.
Van Sweden, B., Wauquier, A., Niedermeyer, E., 1999. Normal aging and transient cognitive disorders in the elderly. In: Electroencephalography: Basic Principles, Clinical Applications, and Related Fields. Lippincott Williams & Wilkins, Baltimore, pp. 340–348.
Villemagne, V.L., Pike, K.E., Chételat, G., Ellis, K.A., Mulligan, R.S., Bourgeat, P., Ackermann, U., Jones, G., Szoeke, C., Salvado, O., 2011. Longitudinal assessment of Aβ and cognition in aging and Alzheimer disease. Ann. Neurol. 69, 181–192.

Vysata, O., Kukal, J., Prochazka, A., Pazdera, L., Valis, M., 2012. Age-related changes in the energy and spectral composition of EEG. Neurophysiology 44, 63–67.
Wang, H.S., Busse, E.W., 1969. EEG of healthy old persons—a longitudinal study. I. Dominant background activity and occipital rhythm 1 2. J. Gerontol. 24, 419–426.
Whalley, L.J., Dick, F.D., McNeill, G., 2006. A life-course approach to the aetiology of late-onset dementias. Lancet Neurol. 5, 87–96.
Yeatman, J.D., Wandell, B.A., Mezer, A.A., 2014. Lifespan maturation and degeneration of human brain white matter. Nat. Commun. 5, 4932.
Zappasodi, F., Marzetti, L., Olejarczyk, E., Tecchio, F., Pizzella, V., 2015. Age-related changes in electroencephalographic signal complexity. PLoS One 10, e0141995.
Zigmond, A.S., Snaith, R.P., 1983. The hospital anxiety and depression scale. Acta psychiatrica Scand. 67, 361–370.